Chemical Science

EDGE ARTICLE

View Article Online
View Journal | View Issue

Cite this: *Chem. Sci.*, 2015, **6**, 6545

Bipyridine complexes of E^{3+} (E = P, As, Sb, Bi): strong Lewis acids, sources of $E(OTf)_3$ and synthons for E^{I} and E^{V} cations†

Saurabh S. Chitnis,[a] Alasdair P. M. Robertson,[a] Neil Burford,*[a] Brian O. Patrick,[b] Robert McDonald[c] and Michael J. Ferguson[c]

Triflate salts of trications $[(bipy)_2E]^{3+}$ ([**6E**][OTf]$_3$) and $[(tbbipy)_2E]^{3+}$ ([**6′E**][OTf]$_3$) (bipy = 2,2′-bipyridine, tbbipy = 4,4′-di-^{t}butyl-2,2′-bipyridine; E = P, As, Sb, Bi) have been synthesized and comprehensively characterized. The unique molecular and electronic structures of this new class of complexes involving pnictogen Lewis acids has been assessed in the solid, solution and gas phases to reveal systematic variations in metric parameters, ligand lability and charge concentration. While the Lewis acidity of E^{3+} has the trend E = Bi < Sb < As < P as determined by gas-phase calculations and ^{1}H NMR spectroscopy, the Lewis acidity of $[\mathbf{6E}]^{3+}$ has the trend E = P < As < Sb < Bi according to gas-phase calculations. Derivatives of [**6′E**][OTf]$_3$ (E = P, As) are latent sources of $E(OTf)_3$ as demonstrated by their reactions with dmap, which give the corresponding derivatives of $[(dmap)_3E][OTf]_3$. The highly oxidizing nature of $P(OTf)_3$ and $As(OTf)_3$ is evidenced in reactions of [**6′E**][OTf]$_3$ (E = P, As) with phosphines, which give E^{I}-containing monocations $[(R_3P)_2E]^{1+}$ and oxidatively coupled dications $[R_3PPR_3]^{2+}$, illustrating new P–P and P–As bond forming strategies. Cations $[\mathbf{6'E}]^{3+}$ (E = P, As) are C–H bond activating agents that dehydrogenate 1,4-cyclohexadiene, with higher activity observed for E = P. Combinations of $[\mathbf{6'E}]^{3+}$ and ^{t}Bu$_3$P activate H_2 and D_2 under mild conditions, evidencing frustrated Lewis pair activity. Oxidation of [**6′P**][OTf]$_3$ with SO_2Cl_2 gives $[(tbbipy)_2PCl_2][OTf]_3$, containing a P^{V}-trication, but there is no evidence of the analogous reaction with [**6′As**][OTf]$_3$. The observations highlight new directions in the chemistry of highly charged cations and reveal a rich reactivity for p-block triflates $E(OTf)_3$, which can be accessed through derivatives of [**6E**][OTf]$_3$ and [**6′E**][OTf]$_3$.

Received 5th July 2015
Accepted 3rd August 2015

DOI: 10.1039/c5sc02423d

www.rsc.org/chemicalscience

Introduction

Numerous monocationic and dicationic p-block element centered complexes are known,[1] but structurally authenticated salts containing trications are rare, because the charge concentration often results in oxidation of the ligands. For example, the trisphosphine-antimony trication **1** (Chart 1) undergoes reductive elimination of a diphosphonium dication below room temperature.[2,3] In this context, the pyridine ligands in **2**,[4] the tris-pyrazole based ligands in **3a,b**,[5] the carbene based ligands in **4a–c**,[6] and the crown ether ligands in **5E**[7] illustrate types of oxidatively resistant donors that enable studies of such reactive coordination centers.

As a prototypical ligand for transition metal acceptors in a variety of oxidation states, 2,2′-bipyridine (bipy) offers relatively high basicity and oxidative resistance, which we have now exploited to enable a comprehensive study of a series of compounds of generic formulae $[(bipy)_2E][OTf]_3$, [**6E**][OTf]$_3$, and $[(tbbipy)_2E][OTf]_3$, [**6′E**][OTf]$_3$ (E = P, As, Sb, Bi; tbbipy = 4,4′-di-^{t}butyl-2,2′-bipyridine).[8] The compounds are characterized as salts containing trications that represent bipy or tbbipy complexes of E^{3+}. A diverse reactivity is evident for these complexes, including ligand exchange, which provides access to the dmap complexes [**7E**][OTf]$_3$ (E = P, As). Element triflates, $E(OTf)_n$, are widely employed as Lewis acids,[9] oxidizing agents[10–12] and latent sources of E^{n+}.[13–15] Interesting examples of small-molecule activation and catalysis effected by p-block element triflate salts are also well documented,[16–18] including those involving $Sb(OTf)_3$ [19] and $Bi(OTf)_3$,[20] which can be isolated on preparative scales,[21,22] enabling their ubiquitous use. Lighter congeners featuring the more electronegative P and As centers have not yet been reported, precluding assessment of their reactivity. In this context, we demonstrate that derivatives of [**6E**][OTf]$_3$ and [**6′E**][OTf]$_3$ represent examples of $E(OTf)_3$ transfer

[a]*Department of Chemistry, University of Victoria, Victoria, British Columbia V8W 3V6, Canada. E-mail: nburford@uvic.ca; Fax: +1 250 721 7147; Tel: +1 250 721 7150*

[b]*Department of Chemistry, University of British Columbia, Vancouver, British Columbia, V6T 1Z1, Canada*

[c]*Department of Chemistry, University of Alberta, Edmonton, Alberta, T6G 2T2, Canada*

† Electronic supplementary information (ESI) available. CCDC 1410568–1410574. For ESI and crystallographic data in CIF or other electronic format see DOI: 10.1039/c5sc02423d

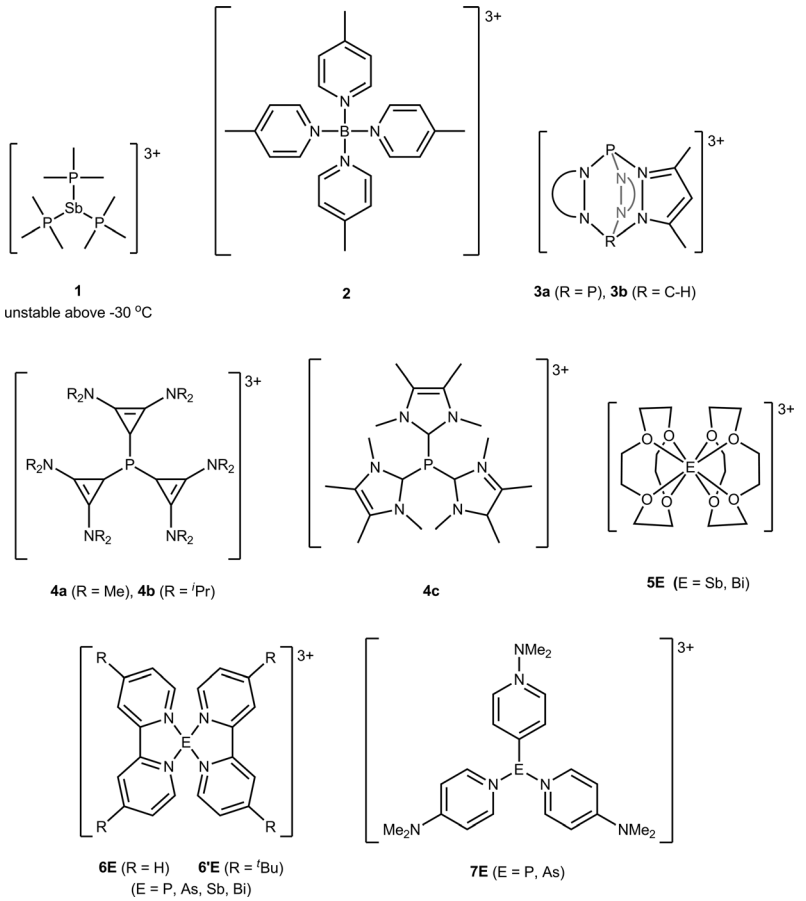

Chart 1 p-Block element centered tricationic complexes.

reagents, C–H and H–H bond activating reagents, and synthons for E^{I}- and E^{V}-centered cations.

Results and discussion

Complexes of $E(OTf)_3$ with bipy or tbbipy were prepared according to Scheme 1 and isolated as crystalline solids. While all derivatives decompose to give the protonated ligand on exposure to ambient atmosphere, they can be stored indefinitely under inert atmosphere at room temperature. Derivatives of [**6E**][OTf]$_3$ are less soluble in MeCN and CH_2Cl_2 than derivatives of [**6′E**][OTf]$_3$, due to the presence of four ^{t}butyl groups in the latter. Interestingly, while the phosphorus derivatives are yellow due to a HOMO–LUMO transition centered around 300 nm,[23] all other derivatives are colourless as solids or in MeCN solutions.

The solid-state structures of [**6P**][OTf]$_3$·2MeCN, [**6′P**][OTf]$_3$·MeCN, [**6′As**][OTf]$_3$·2.83MeCN, [**6Sb**][OTf]$_3$·MeCN, [**6′Sb**][OTf]$_3$·MeCN, and [**6Bi**][OTf]$_3$·MeCN have been determined to reveal spirocyclic environments for E with four E–N bonds (10-E-4 as per the Arduengo nomenclature[24]) and varying degrees of E–O triflate contacts, as shown in Fig. 1. Selected metric parameters for derivatives of [**6E**][OTf]$_3$ and [**6′E**][OTf]$_3$ are collated in Table 1, where computationally determined (gas phase) values are listed for [**6As**]$^{3+}$ and [**6′Bi**]$^{3+}$, for which experimental solid state data are not available. In all cases, the structures indicate the stereochemical presence of a lone pair at the acceptor pnictogen centre. The intermolecular MeCN···P interaction for [**6′P**][OTf]$_3$·MeCN (coordinated solvent) and interion O···E interactions (triflate anions) in [**6P**][OTf]$_3$, [**6′P**][OTf]$_3$·MeCN, [**6′As**][OTf]$_3$·2.83MeCN, and [**6′Sb**][OTf]$_3$·MeCN are closer in magnitude to $\sum_{r,vdW}$ than to $\sum_{r,cov}$ for the elements involved. In contrast, short Bi···O interactions are observed in [**6Bi**][OTf]$_3$, representing elongated Bi–O covalent bonds rather than triflate anions interacting with a bismuth cation. We therefore classify all derivatives as ionic except [**6Bi**][OTf]$_3$ which is best described in the solid state as a bis-bipy adduct of $Bi(OTf)_3$.

The bond angles for a given E in [**6E**][OTf]$_3$ and [**6′E**][OTf]$_3$ are expected to be very similar because the divergent planes defined by N_1–E–N_2 and N_3–E–N_4 result in the ^{t}Bu groups facing away from each other, so that steric repulsion between them is

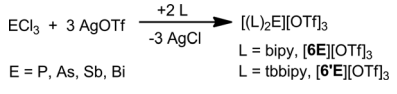

Scheme 1 Synthesis of [**6E**][OTf]$_3$ and [**6′E**][OTf]$_3$.

minimal. For example, the quaternary carbon centers in the ^{t}Bu groups that are *para* to N_2 and N_4 in [**6′P**][OTf]$_3$ are separated by nearly 10 Å, and the bond angles within the disphenoidal frames of [**6P**]$^{3+}$ and [**6′P**]$^{3+}$ are essentially identical, as they are for [**6Sb**]$^{3+}$ and [**6′Sb**]$^{3+}$. The inductive effect of a ^{t}Bu group *para* to the nitrogen atoms is expected to make the tbbipy ligands more basic compared to bipy and lead to stronger E–N interactions. Consistently, the ^{31}P NMR spectrum of a CD_3CN mixture containing tbbipy and [**6P**][OTf]$_3$ in a 2 : 1 stoichiometry showed a broad peak corresponding to [**6P′**][OTf]$_3$. The E–N distances in [**6P**][OTf]$_3$·2MeCN and [**6′P**][OTf]$_3$·MeCN are similar, although the presence of a coordinated MeCN donor in the latter may reduce the electrophilicity of the phosphorus center and offset the expected E–N shortening. Better suited for direct comparison are [**6Sb**][OTf]$_3$·MeCN and [**6′Sb**][OTf]$_3$·MeCN, where the MeCN molecule in the lattice does not interact with the Sb centers. Evidencing the inductive effect of the *para*-^{t}Bu group, E–N distances in [**6′Sb**][OTf]$_3$·MeCN are on average 0.1 Å shorter than the bipy derivative, which also shows two more Sb–O interion contacts than does the tbbipy derivative. Moreover, the Sb–O contacts in [**6′Sb**][OTf]$_3$·MeCN are on average 0.05 Å longer than those in [**6Sb**][OTf]$_3$·MeCN. These observations support a slightly greater Lewis basicity for tbbipy, which is discernible in the E–N distances, in the absence of additional donors (*e.g.* coordinated solvent) at E.

The *trans* configured E–N bonds in all derivatives are *ca.* 0.1 Å longer than the E–N bonds in equatorial positions due to the mutual *trans* influence of the E–N_1 and E–N_3 interactions (Fig. 2). For the equatorial positions, the trend in E–N bond lengths, [**6P**]$^{3+}$ ≈ [**6′P**]$^{3+}$ < [**6′As**]$^{3+}$ < [**6Sb**]$^{3+}$ ≈ [**6′Sb**]$^{3+}$ < [**6Bi**]$^{3+}$, reflects the sum of the respective covalent radii ($\sum_{r,cov}$). The trend in the axial (N_1–E–N_3) and equatorial interligand angles (N_2–E–N_4), [**6P**]$^{3+}$ ≈ [**6′P**]$^{3+}$ > [**6′As**]$^{3+}$ > [**6Sb**]$^{3+}$ ≈ [**6′Sb**]$^{3+}$ > [**6Bi**]$^{3+}$, is consistent and is attributed to the extent of triflate

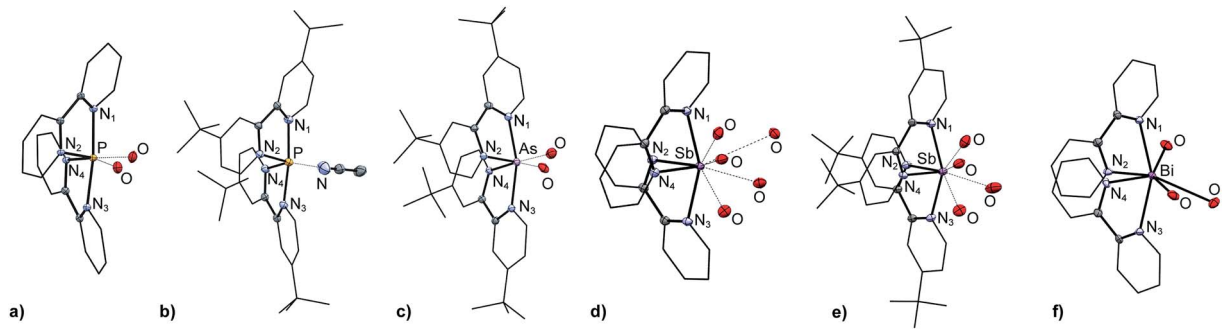

Fig. 1 Solid-state molecular structures of the cations in (a) [**6P**][OTf]$_3$·2MeCN, (b) [**6′P**][OTf]$_3$·MeCN, (c) [**6′As**][OTf]$_3$·2.83MeCN, (d) [**6Sb**][OTf]$_3$·MeCN, (e) [**6′Sb**][OTf]$_3$·MeCN, and (f) [**6Bi**][OTf]$_3$. Hydrogen atoms, non-interacting portions of the triflate anions and solvent molecules have been omitted for clarity.

Table 1 Selected bond lengths (Å) and angles (°) in the solid-state structures of [**6P**][OTf]$_3$·2MeCN, [**6′P**][OTf]$_3$·MeCN, [**6′As**][OTf]$_3$·2.83MeCN, [**6Sb**][OTf]$_3$·MeCN,[8] [**6′Sb**][OTf]$_3$·MeCN, and [**6Bi**][OTf]$_3$, calculated (gas phase, PBE0/def2-TZVP) values for cations [**6As**]$^{3+}$ and [**6′Bi**]$^{3+}$, and sums of covalent ($\sum_{r,cov}$)[25] and van der Waals ($\sum_{r,vdW}$)[26,27] radii for selected atom pairs

	[**6P**][OTf]$_3$·2MeCN	[**6′P**][OTf]$_3$·MeCN	[**6As**]$^{3+}$	[**6′As**][OTf]$_3$·2.83MeCN	[**6Sb**][OTf]$_3$·MeCN	[**6′Sb**][OTf]$_3$·MeCN	[**6Bi**][OTf]$_3$·MeCN	[**6′Bi**]$^{3+}$
E–N_1	1.939(2)	1.971(2)	2.0993	2.124(2)	2.284(2)	2.269(2)	2.454(6)	2.3461
E–N_2	1.811(2)	1.812(2)	1.9714	1.997(2)	2.233(2)	2.198(2)	2.364(6)	2.2519
E–N_3	1.974(2)	1.959(2)	2.0993	2.125(2)	2.332(2)	2.310(2)	2.430(6)	2.3461
E–N_4	1.816(2)	1.811(2)	1.9714	1.999(2)	2.243(2)	2.218(2)	2.372(6)	2.2519
$\sum_{r,cov}$(E, N)	1.82	1.82	1.92	1.92	2.11	2.11	2.22	2.22
$\sum_{r,vdW}$(E, N)	3.35	3.35	3.40	3.40	3.61	3.61	3.62	3.62
E–O_{OTf}	3.006(2)		—	2.705(2)	2.598(2)	2.586(2)	2.607(6)	—
	3.109(2)			2.742(2)	2.650(2)	3.113(2)	2.532(6)	
					3.077(1)	2.767(2)	2.893(6)	
					3.247(1)	3.343(2)		
					3.367(1)			
$\sum_{r,cov}$(E, O)	1.74	1.74	1.84	1.84	2.03	2.03	2.14	2.14
$\sum_{r,vdW}$(E, O)	3.32	3.32	3.37	3.37	3.58	3.58	3.59	3.59
N_1–E–N_2	82.20(7)	81.61(8)	78.86	77.67(8)	72.09(4)	72.43(5)	68.1(2)	71.53
N_3–E–N_4	82.07(7)	82.25(8)	78.86	77.76(8)	71.53(4)		68.2(2)	71.53
N_1–E–N_3	173.09(8)	173.10(8)	168.47	162.75(8)	156.02(4)	153.45(5)	154.4(2)	152.92
N_1–E–N_4	92.91(7)	92.63(8)	93.47	89.96(8)	87.87(4)	89.17(5)	94.1(2)	90.16
N_2–E–N_3	93.36(7)	94.44(8)	93.47	90.45(8)	91.42(4)	86.70(5)	88.8(2)	90.16
N_2–E–N_4	99.57(8)	97.56(8)	97.39	91.54(8)	78.66(4)	81.98(5)	74.7(2)	95.78

anion association, which is greater for an atom with a larger atomic radius. The chelation angles ($N_{1/3}$–E–$N_{2/4}$) exhibit the trend $[\mathbf{6P}]^{3+} \approx [\mathbf{6'P}]^{3+} > [\mathbf{6'As}]^{3+} > [\mathbf{6Sb}]^{3+} \approx [\mathbf{6'Sb}]^{3+} > [\mathbf{6Bi}]^{3+}$ as the N–E–N interaction subtends smaller angles for longer E–N bonds.

Infrared spectra for derivatives of $[\mathbf{6'E}][OTf]_3$ enable quantification of the interion coordination in the solid state. The symmetric SO_3 stretch, $\nu_s(SO_3)$, in several triflate salts has been studied previously and appears as a characteristically sharp absorbance in the 1020–1050 cm^{-1} range.[28] The portions of the infrared spectra of $[\mathbf{6'E}][OTf]_3$ shown in Fig. 3 illustrate a trend in $\nu(SO_3)$ of E = P > As > Sb > Bi, which we attribute to the degree of charge transfer from the anion to the pnictogen centre, which influences the S–O bond order. The broader bands for the heavier homologues are attributed to the loss of C_{3v} symmetry due to cation–anion interaction. The spectra for ligand-free $Sb(OTf)_3$ and $Bi(OTf)_3$, for which extensive Sb–O and Bi–O interactions are predicted, exhibit similarly broad S–O stretching bands (see Fig. S2, ESI†) that are shifted to lower frequencies (958 cm^{-1} and 1000 cm^{-1}, respectively) than the analogous value in $[Bu_4N][OTf]$ (1032 cm^{-1}),[28] which features a weakly coordinating cation, and the calculated value for an isolated triflate anion in the gas phase (1035 cm^{-1}, PBE0/aug-cc-pVTZ).

Gas-phase structures, bonding, and Lewis acidity of $[\mathbf{6E}]^{3+}$

Optimized structures for $[\mathbf{6E}]^{3+}$ in the gas phase adopt a disphenoidal C_2 symmetry for all derivatives, consistent with the observed solid-state structures. Selected calculated bond lengths and angles are given in Table 2. As observed experimentally in the solid state, the computed structures reveal axial E–N distances that are longer by *ca.* 0.1 Å than the equatorial E–N distances and average E–N bond distances that are primarily determined by the respective covalent radii. For pnictogen centers with a larger covalent radius, the bite angle $N_{1/3}$–E–$N_{2/4}$ and the equatorial and the axial interligand angles are smaller. The equatorial interligand angle in the solid-state structures of Sb and Bi derivatives are significantly smaller than in the anion-free gas-phase structures of $[\mathbf{6Sb}]^{3+}$ and $[\mathbf{6Bi}]^{3+}$, suggesting that the steric pressure of the interion contacts present in the solid state influence this angle. By comparison the axial interligand angle N_1–E–N_3 in the experimental and calculated structures are essentially identical, implying minimal distortion due to interion contacts.

Natural Bond Orbital (NBO) partial charges and Wiberg Bond Indices (WBI) for the gas-phase cations are listed in Table 3, evidencing a high positive charge for the central pnictogen centre, which is greater for heavier elements, as expected on the basis of relative electronegativities. Consistently, the WBIs for the N–E interaction has the trend P > As > Sb > Bi, implying a more ionic E–N bond for the heavier pnictogens. For a given derivative, the WBI value for the axial E–N interactions is smaller than the equatorial interactions, indicating less effective bonding along the N_1–E–N_3 axis than in the N_2–E–N_4 plane. Noting that the equatorial interligand angles range from 95 to 100° in all cases, we surmise that of the three mutually perpendicular p-orbitals that serve as acceptor orbitals at E^{3+}, two are engaged by N_2 and N_4 in the equatorial plane, while the third accommodates two strained *trans* interactions involving N_1 and N_3.

To assess the relative Lewis acidities of E^{3+}, we have calculated the enthalpies for the heterolytic removal of both bipy ligands from $[\mathbf{6E}]^{3+}$. Scheme 2a represents removal of the ligands and relaxation of their geometries to the C_{2h} minimum for free bipy, and Scheme 2b represents removal of the ligands with retention of the geometry observed in $[\mathbf{6E}]^{3+}$. The difference between the two enthalpies represents the energy required for two non-interacting bipy molecules (C_{2h}) to adopt the $(bipy)_2$ geometry in each complex (Scheme 2c). The ΔH_{rxn} values in Table 4 show that the enthalpic requirement for ligand dissociation from E^{3+} has the trend E = Bi < Sb < As < P, irrespective of whether or not steric factors are considered. Values for ligand strain show a parallel trend, but the range (98–181 kJ mol^{-1}) is small compared to the range for the overall ligand dissociation process (2302–3575 kJ mol^{-1}). We therefore conclude that steric

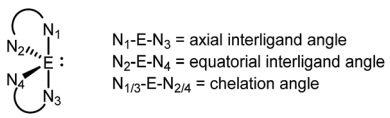

Fig. 2 Definition of key angles in the disphenoidal geometry of $[\mathbf{6E}]^{3+}$.

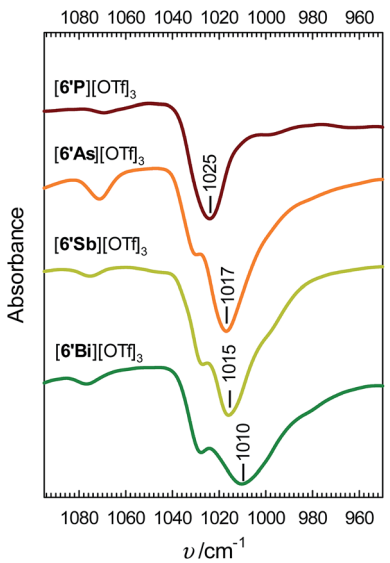

Fig. 3 Infrared spectra (950–1100 cm^{-1}) of $[\mathbf{6'E}][OTf]_3$ obtained on powdered salts using an ATR module.

Table 2 Select bond lengths and angles in the calculated (gas-phase, PBE0/def2-TZVP) structures of cations $[\mathbf{6E}]^{3+}$. See Fig. 2 for numbering scheme

Cation	$N_{1/3}$–E	$N_{2/4}$–E	$N_{1/3}$–E–$N_{2/4}$	N_2–E–N_4	N_1–E–N_3
$[\mathbf{6P}]^{3+}$	1.9511	1.8224	82.72	100.61	175.68
$[\mathbf{6As}]^{3+}$	2.0993	1.9714	78.86	97.39	168.47
$[\mathbf{6Sb}]^{3+}$	2.2545	2.1677	73.96	95.19	157.34
$[\mathbf{6Bi}]^{3+}$	2.3607	2.2678	71.50	95.12	153.59

Table 3 Calculated (PBE0/def2-TZVP) NBO partial charges and Wiberg bond indices for $[\mathbf{6E}]^{3+}$ in the gas phase. See Fig. 2 for numbering scheme

E	Charge (E)	Charge ($N_{1/3}$)	Charge ($N_{2/4}$)	WBI ($N_{1/3}$–E)	WBI ($N_{2/4}$–E)
P	+1.40	−0.53	−0.52	0.49	0.69
As	+1.58	−0.54	−0.54	0.43	0.61
Sb	+1.78	−0.55	−0.56	0.39	0.58
Bi	+1.86	−0.54	−0.55	0.36	0.50

effects have a minor influence on the calculated enthalpies of ligand dissociation in Scheme 2a, which are dominated by electronic effects.

We rationalize the calculated trend in dissociation enthalpies on the basis of atomic size, with a smaller atom having a higher charge concentration and the best orbital match in the N(sp^3)→E(np) HOMO–LUMO interaction (*cf.* N(sp^3)→P(3p) *vs.* As(4p) *vs.* Sb(5p) *vs.* Bi(6p)). The electrostatic and orbital interactions are both expected to weaken as atomic radii and the number of nodes in the acceptor p-orbitals increase. The trend in ligand strain is presumably related to the N_1–E–N_3 angle, which shows the most dramatic variation amongst all parameters in the calculated structures of $[\mathbf{6E}]^{3+}$, and decreases over a 22° range from phosphorus (175.68°) to bismuth (153.59°). We propose that the strained ligand geometry in $[\mathbf{6P}]^{3+}$ is enforced by orbital interactions involving three mutually perpendicular 3p acceptor orbitals at the P^{3+} centre. By comparison, in $[\mathbf{6Bi}]^{3+}$, where E–N bonding is calculated to be more ionic (Table 3), the preference for an N_1–E–N_3 angle of 180° is lowest.

Table 4 Calculated (PBE0/def2-TZVP) reaction enthalpies (kJ mol^{-1}, 298 K, gas phase) for the processes in Scheme 2a–d

E	ΔH_{rxn} (Scheme 2a)	ΔH_{rxn} (Scheme 2b)	ΔH_{rxn} (Scheme 2c)	ΔH_{rxn} (Scheme 2d)
P	3575	3756	181	178
As	3127	3264	137	210
Sb	2539	2649	110	244
Bi	2302	2400	98	255

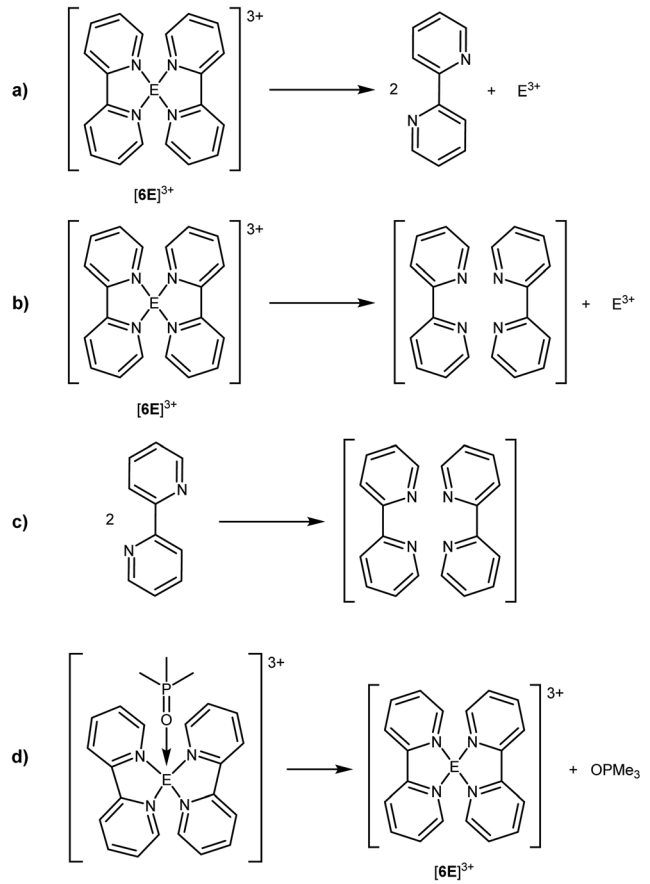

Scheme 2 (a) Dissociation of two bipy ligands in $[\mathbf{6E}]^{3+}$, (b) dissociation of two bipy ligands in $[\mathbf{6E}]^{3+}$ with retention of the $(bipy)_2$ geometry of $[\mathbf{6E}]^{3+}$, (c) organization of two bipy ligands to the $(bipy)_2$ geometry found in $[\mathbf{6E}]^{3+}$, and (d) dissociation of $OPMe_3$ from $[(bipy)_2E(OPMe_3)]^{3+}$.

While reaction enthalpies for Scheme 2a and b represent the Lewis acidity of monoatomic trications E^{3+}, ΔH_{rxn} for Scheme 2d assesses the Lewis acidities of complexes $[\mathbf{6E}]^{3+}$ by measuring the energy required for removal of a prototypical ligand, $OPMe_3$, from hypothetical complexes $[(bipy)_2E(OPMe_3)]^{3+}$. The enthalpies for this process indicate that the Lewis acidity of complexes $[\mathbf{6E}]^{3+}$ has the trend E = P < As < Sb < Bi, which is the opposite trend to that of monoatomic E^{3+}, and is rationalised on steric grounds acknowledging the trend in atomic radii and consequential coordination sphere. Consistently, the range of enthalpy values calculated for Scheme 2d (178–255 kJ mol^{-1}) is much smaller than that observed for Scheme 2a (2302–3575 kJ mol^{-1}) and is comparable to the ligand strain enthalpies calculated for Scheme 2c (98–181 kJ mol^{-1}). In addition, comparison of the optimized structures for $[\mathbf{6E}]^{3+}$ and $[(bipy)_2E(OPMe_3)]^{3+}$ shows that the greatest geometric deformation upon complexation with $OPMe_3$ is compression of the interligand angle N_2–E–N_4 (see Fig. 2 for definition). The magnitude of this geometric adjustment, which leads to steric clash between the bipy ligands, is greatest for E = P (15°) and least for E = Bi (7°), consistent with the calculated trend for Scheme 2d.

NMR characterization of $[\mathbf{6E}][OTf]_3$ and $[\mathbf{6'E}][OTf]_3$

CD_3CN solutions of $[\mathbf{6E}][OTf]_3$ and $[\mathbf{6'E}][OTf]_3$ exhibit ^{19}F NMR chemical shift values for all species in the range −78.9 to −79.5 ppm (*cf.* −79.4 for $[PPh_4][OTf]$), indicative of dissociated triflate ions. In addition, solutions of all derivatives polymerize THF within hours of mixing, implicating a high Lewis

acidity[29,30] in coordinating solvents. No significant change was observed in the ^{1}H or ^{31}P NMR shifts of salts [**6′E**][OTf]$_3$ over a broad concentration range, implying the absence of a bimolecular association process as might be expected from an equilibrium between the anion-bound and anion-free cations (see representative data for [**6′Bi**][OTf]$_3$ in Fig. S3, ESI†). We conclude that CD_3CN solutions of [**6E**][OTf]$_3$ and [**6′E**][OTf]$_3$ contain solvated trications and triflate anions with minimal interion interaction.

The aromatic resonances in the ^{1}H NMR spectra of derivatives of [**6E**][OTf]$_3$ in CD_3CN are shown in Fig. 4. As predicted for a C_2 symmetric bis-bipy complex, eight aromatic resonances are detected for [**6P**][OTf]$_3$ at 25 °C. For [**6As**][OTf]$_3$, four broad peaks are observed, which broaden further upon cooling to 0 °C and resolve into additional peaks upon cooling to −35 °C. Only four aromatic resonances are detected for [**6Sb**][OTf]$_3$ and [**6Bi**][OTf]$_3$, at 25 °C and at −35 °C. While the solid-state structure, featuring eight unique hydrogen environments for the cations in [**6E**][OTf]$_3$ (Fig. 1), is apparently retained in solution for E = P, the mobility of the bipy ligands at 25 °C is sufficiently high for E = As, Sb, and Bi that only four hydrogen environments are detected. At −35 °C, ligand mobility is partially restricted for [**6As**][OTf]$_3$ leading to additional signals but complete resolution of eight hydrogen environments, as in [**6P**][OTf]$_3$, was not detected. The observations indicate a mobility for the bipy ligands around E with the trend E = P < As < Sb ≈ Bi and parallels the trend in ionicity for the E–N bond (Table 3). We propose that the more covalent N–P and N–As bonds are conformationally rigid due to the directional requirements of efficient orbital overlap to make a covalent bond (three mutually perpendicular p-orbitals), whereas the more ionic N–Sb and N–Bi interactions

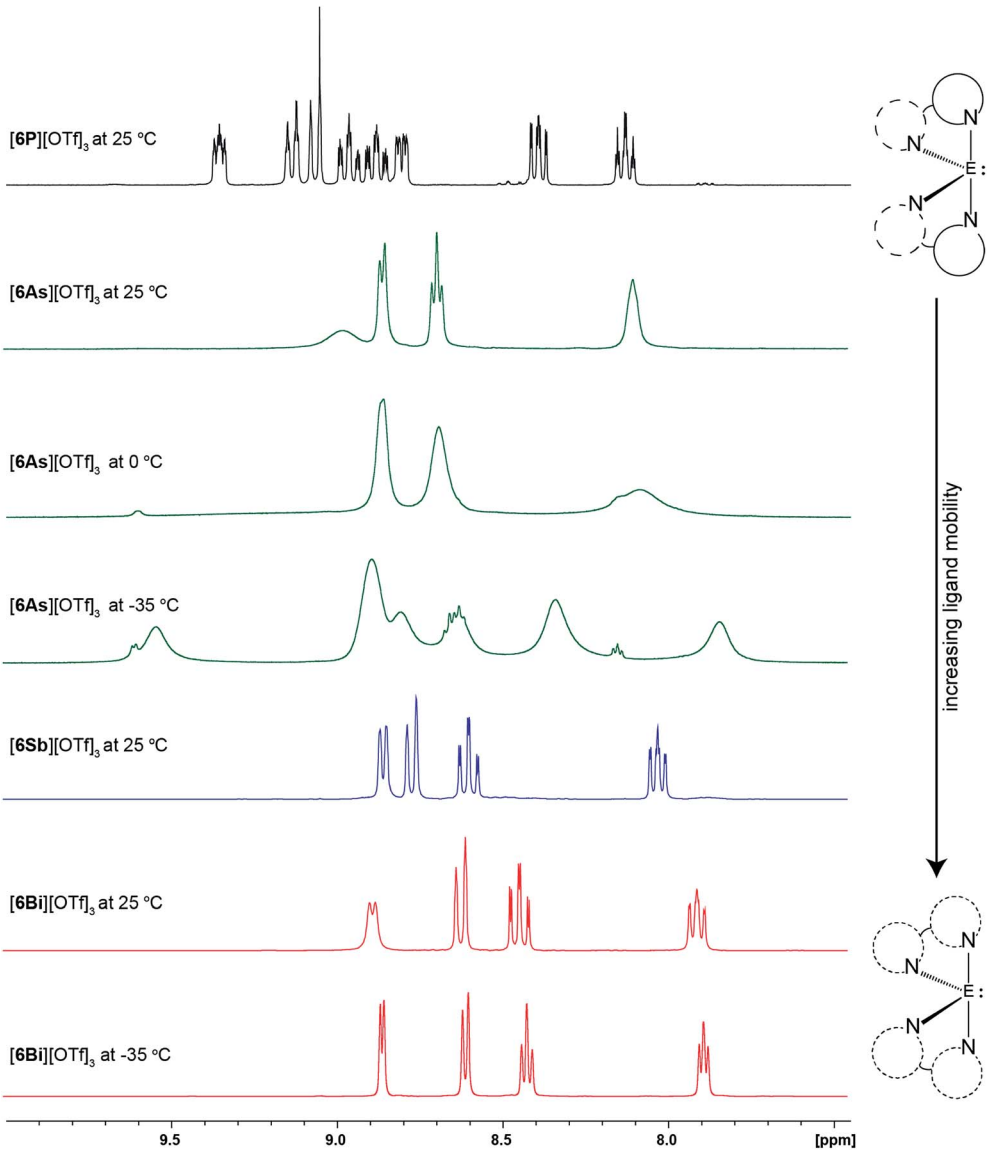

Fig. 4 ^{1}H NMR resonances in the aromatic region for CD_3CN solutions of [**6P**][OTf]$_3$ (black), [**6As**][OTf]$_3$ (green), [**6Sb**][OTf]$_3$ (blue), and [**6Bi**][OTf]$_3$ (red).

have a smaller barrier to motion due to the absence of a directional component for electrostatic interactions (point charges).

The difference between the ^{31}P NMR chemical shift of free Et_3PO and that of its adduct with a Lewis acid has been correlated with the strength of the Lewis acid (Gutmann–Beckett method).[31,32] No systematic trend was observed in the chemical shifts observed (see Fig. S4, ESI†) in ^{31}P NMR assays of solutions containing equimolar amounts of Et_3PO and [**6′E**][OTf]$_3$.[33] Moreover, in the case of [**6′P**][OTf]$_3$, a complex spectrum showing a mixture of products was obtained, none of which could be assigned to the phosphine oxide adduct. Deoxygenation of Et_3PO by electrophilic phosphorus cations has been reported recently and may be operative.[34] Moreover, as a wide range in covalent radii (1.11–1.51 Å)[25] is spanned going from P to Bi, the steric influence on ^{31}P chemical shifts may be greater than those due to differing Lewis acidities, confounding a straightforward assessment due to steric factors, as highlighted recently for borane Lewis acids.[35]

Reactivity of [6′P][OTf]$_3$ and [6′As][OTf]$_3$

The structures of [**6P**][OTf]$_3$ and [**6′P**][OTf]$_3$ represent rare examples of hypervalent phosphorus(III) acceptor centres, and are comparable to those involving N-heterocyclic carbene (NHC),[36] phosphine,[37,38] catecholate,[39] and phenylpyrazole[40] ligands. Moreover, electron precise (8 valence electron) phosphorus based frameworks **3** and **4** (Chart 1) are the only phosphorus(III) centred trications that have been structurally characterized.[41] By comparison, the 10 valence electron count imposed by the two chelate ligands at phosphorus in [**6P**]$^{3+}$ and [**6′P**]$^{3+}$ render these trications as novel examples of electron-rich phosphorus Lewis acids. Examples of arsenic(III)-centred mono- and dications featuring phosphine[42] or bipy[43] ligands have been reported as well as two-coordinate arsenium monocations.[44–46] However, [**6′As**][OTf]$_3$ is the first structurally authenticated example of an arsenic-centred trication.

The reactivity of Sb(OTf)$_3$ and Bi(OTf)$_3$ has been studied previously, leading to their widespread use as Lewis acid catalysts,[19,20] but the absence of synthetic routes to P(OTf)$_3$ and As(OTf)$_3$ has precluded investigations of these potential synthetic reagents. Phosphorus polycations have been used as a precursors to cationic bicyclophosphines and cyclic phosphorus oxides,[47] and derivatives of **4** (Chart 1) have been shown to bind transition metal centers *via* the lone pair at the phosphorus(III) center to give highly effective pre-catalysts for C–C bond forming reactions.[48] Intrigued by the unique intersection of molecular and electronic structures represented by the trications in [**6′P**][OTf]$_3$ and [**6′As**][OTf]$_3$, and envisioning these salts as *in situ* equivalents of E(OTf)$_3$ (E = P, As), we have conducted an initial survey of their reactivity.

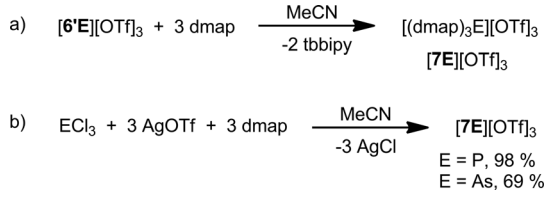

Scheme 3 (a) Formation of [**7E**][OTf]$_3$ from [**6′E**][OTf]$_3$. (b) Independent synthesis of [**7E**][OTf]$_3$ (E = P, As).

[6′E][OTf]$_3$ as E(OTf)$_3$ transfer reagents

Reactions of [**6′E**][OTf]$_3$ (E = P, As) with three equivalents of 4-dimethylaminopyridine (dmap) quantitatively (by ^{31}P and ^{1}H NMR) yield [(dmap)$_3$E][OTf]$_3$, [**7E**][OTf]$_3$, (E = P, As) and free tbbipy (Scheme 3a). Neither dmap complexes could be isolated from the reaction mixtures but their identities were definitively established by independent syntheses (Scheme 3b) and structural elucidation (Fig. 5). While the [**7P**]$^{3+}$ ion has previously been detected spectroscopically in mixtures of PCl_3 and dmap,[49,50] the ^{31}P NMR chemical shift attributed to the trichloride salt was reported to vary widely (δ = 79–114 ppm) depending upon concentration, suggesting a dynamic process.[51] By comparison, [**7P**][OTf]$_3$ exhibits a ^{31}P NMR chemical shift (δ = 101.7 ppm) for the redissolved crystals that does not vary over a broad concentration range.

The solid-state structures of [**7E**][OTf]$_3$ reveal three dmap ligands bound to the pnictogen centers giving a trigonal pyramidal geometry at the pnictogen centre for the [**7E**]$^{3+}$ ions.[52] Three weak contacts with the triflate anions are evident, giving a six-coordinate geometry that is distorted by the

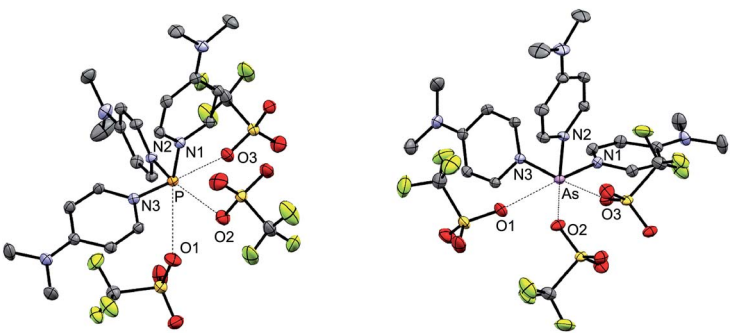

Fig. 5 Solid state structures of [**7P**][OTf]$_3$·1.5MeCN (left, one of two crystallographically distinct molecules shown) and [**7As**][OTf]$_3$·2MeCN (right). Hydrogen atoms and solvent molecules have been omitted for clarity.

presence of a stereochemically active lone pair in each case. The three weak E···O contacts are *trans* configured with respect to the three E–N bonds. The E–N bond lengths (Table 5) reflect the relative atomic radii of the phosphorus and arsenic atoms and are 0.1–0.2 Å shorter than the corresponding values in [**6P**][OTf]$_3$, [**6′P**][OTf]$_3$, and [**6′As**][OTf]$_3$ due to the greater basicity and lesser steric demands of dmap compared to bipy or tbbipy. The N–E–N bond angles in [**7E**][OTf]$_3$ are in the 90–100° range consistent with values observed for the *cis*-configured N–E–N angles in derivatives of [**6E**][OTf]$_3$ and [**6′E**][OTf]$_3$ (Table 5).

[6′E]$^{3+}$ as synthons for E^{I} cations

In contrast to ligand exchange with dmap, reaction of [**6′P**][OTf]$_3$ with PMe_3 yields products due to redox chemistry (Scheme 4a). The previously reported P^{I} containing reduction product, $[(Me_3P)_2P]^{1+}$ (δ = 15.0 and −156.3 ppm, $^1J_{PP}$ = 438 Hz)[53] and the P^{IV} containing oxidation product, $[Me_3PPMe_3]^{2+}$ (δ = 28.4 ppm),[54] have been definitively identified by ^{31}P NMR spectroscopy (Fig. S5, ESI†). The analogous reaction with PPh_3 yielded $[(Ph_3P)_2P]^{1+}$ (δ = 30, −174, $^1J_{PP}$ = 502 Hz)[55] as the major product, but a complex mixture of oxidation products was obtained, suggesting that $[Ph_3PPPh_3]^{2+}$, which is isoelectronic with the metastable hexaphenylethane molecule,[56] may also be unstable relative to its constitutional isomers (Scheme 4b). Similarly, a ^{31}P NMR assay of the 1 : 3 reaction between [**6′As**][OTf]$_3$ and PMe_3 showed a singlet due to $[Me_3PPMe_3]^{2+}$ together with a resonance at 22.4 ppm, tentatively assigned to the As^{I} cation, $[(Me_3P)_2As]^{1+}$, which could not be isolated from the reaction mixture (Scheme 4c). In a parallel experiment, a ^{31}P NMR assay of the 1 : 2 reaction between [**6′As**][OTf]$_3$ and 1,2-bis(diphenylphosphino)ethane (dppe) showed a singlet at 60.5 ppm due to the previously reported As^{I} cation $[(dppe)As]^{1+}$,[57] and unidentified oxidation products (Scheme 4d). We conclude that trications [**6′E**]$^{3+}$ are strong oxidizing agents owing to their formidable molecular charge and effect oxidative P–P coupling while being reduced to P^{I} or As^{I} containing monocations. This redox outcome contrasts the ligand displacement observed in the presence of the more oxidatively resistant ligand dmap, and is analogous to reactivity patterns established for $FSb(OTf)_2$ and $Sb(OTf)_3$.[21]

Table 5 Selected bond lengths (Å) and angles (°) in the solid-state structures of [**7P**][OTf]$_3$·1.5MeCN and [**7As**][OTf]$_3$·2MeCN

	[**7P**][OTf]$_3$·1.5MeCN	[**7As**][OTf]$_3$·2MeCN
E–N$_1$	1.7635(17)	1.9157(17)
E–N$_2$	1.7578(16)	1.9447(16)
E–N$_3$	1.7588(17)	1.9174(16)
E–O$_{Otf}$	3.0462(18)	2.8428(15)
	3.2615(17)	2.654(2)
	3.0395(19)	2.969(2)
N$_1$–E–N$_2$	98.42(8)	92.51(7)
N$_2$–E–N$_3$	97.40(8)	92.64(7)
N$_1$–E–N$_3$	99.24(8)	96.45(7)

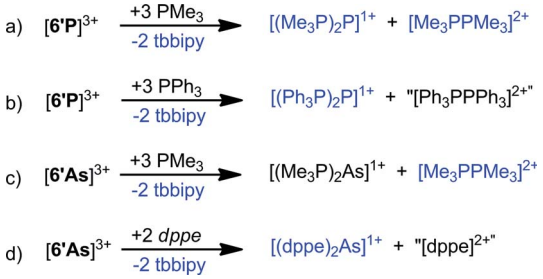

Scheme 4 Reactions of [**6′E**][OTf]$_3$ (E = P, As) with phosphines. Species in blue were definitively identified by their previously reported ^{1}H or ^{31}P NMR resonances.

C–H and H–H bond activation by [6′E]$^{3+}$

The equimolar reaction of [**6′P**][OTf]$_3$ with 1,4-cyclohexadiene in CD_3CN showed complete consumption of starting materials after 16 hours at 80 °C (Scheme 5a). The ^{1}H NMR of the reaction mixture showed formation of benzene (δ = 7.38 ppm) and diprotonated tbbipy as the major products (>80%, Fig. S6, ESI†). The ^{31}P NMR spectrum exhibits a mixture of unidentified products, none of which exhibit P–H couplings. The spectroscopic data are consistent with C–H bond activation involving dehydrogenation of 1,4-cyclohexadiene and sequestering of protons in [tbbipy-H$_2$]$^{2+}$. The analogous reaction with [**6′As**][OTf]$_3$ showed only 10% conversion of 1,4-cyclohexadiene to benzene over 16 h at 80 °C, with concomitant formation of [tbbipy-H$_2$]$^{2+}$ and an insoluble black precipitate (Fig. S7, ESI†). C–H bond activation has recently been reported for mixtures of diphosphonium dications and ^{t}Bu$_3$P.[58] Consistently, the 1 : 2 combinations of [**6′E**][OTf]$_3$ (E = P, As) and ^{t}Bu$_3$P in CD_3CN effect complete dehydrogenation of 1,4-cyclohexadiene to yield benzene and [^{t}Bu$_3$P-H]$^{1+}$ within 16 hours at 80 °C (Scheme 5b). In line with the expectation that these reactions proceed *via* formation of a frustrated Lewis pair[59] between [**6′E**]$^{3+}$ and ^{t}Bu$_3$P, ^{31}P NMR spectra of equimolar reaction mixtures containing ^{t}Bu$_3$P and either [**6′P**][OTf]$_3$ or [**6′As**][OTf]$_3$ show no evidence of coordination between the strong Lewis acids and the bulky base pairs (see Fig. S8, ESI†). Frustrated Lewis pair activity is also evidenced by 1 : 2 mixtures of [**6′P**][OTf]$_3$ and ^{t}Bu$_3$P in CD_3CN with H_2 or D_2 (1 atm pressure) in a sealed NMR tube at 80 °C over 16 hours (Scheme 5c), which show complete conversion of ^{t}Bu$_3$P to [^{t}Bu$_3$P-H]$^{1+}$ or [^{t}Bu$_3$P-D]$^{1+}$ by ^{31}P NMR spectroscopy (Fig. S9, ESI†).

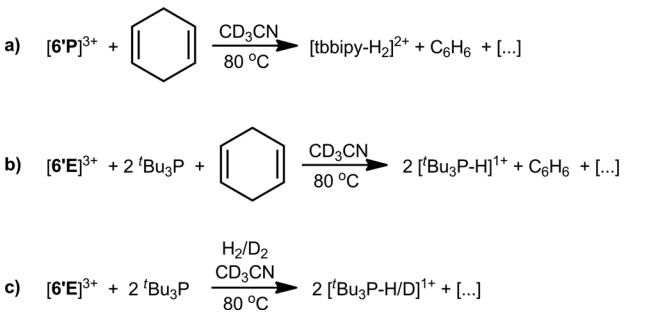

Scheme 5 C–H and H–H bond activation by [**6′E**][OTf]$_3$.

$[6'E]^{3+}$ as synthons for E^V cations

The ^{31}P NMR spectrum of an equimolar mixture of $[6'P][OTf]_3$ and SO_2Cl_2 shows a single ^{31}P NMR resonance at $\delta = -146.9$ ppm, assigned to the P^V containing $[(tbbipy)_2PCl_2]^{3+}$. The upfield resonance is consistent with a five- or six-coordinate geometry and is similar to shifts reported for $[(dmap)_2PCl_4]^{1+}$ ($\delta = -196$ ppm)[60] and $[(bipy)PCl_4]^{1+}$ ($\delta = -191$ ppm).[61] Moreover, the singlet at −146.9 ppm is also observed in the ^{31}P NMR spectrum of a 2 : 1 : 3 mixture of tbbipy, PCl_5 and TMSOTf.

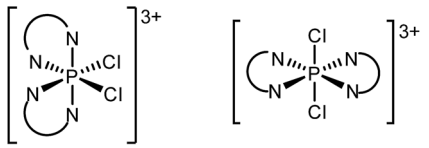

cis *trans*

Two configurational outcomes are envisioned for the octahedral structure of $[(tbbipy)_2PCl_2]^{3+}$, with a *cis* or *trans* arrangement of the chlorine atoms. The ^1H NMR spectrum of the cation shows six resonances in the aromatic region (Fig. 6) and two resonances for the ^{t}Bu groups, consistent with C_2 symmetry, precluding a *trans* configuration of chlorine centres. Gas-phase calculations using bipy ligands revealed that both isomers are true energy minima (no negative vibrational frequencies), but a 64 kJ mol^{-1} preference for the *cis* isomer was calculated, arising from significant steric clash between the *ortho* hydrogen atoms of the ligands when a *trans* configuration is imposed (Fig. S10, ESI†). No *cis*/*trans* isomerism was detected experimentally upon heating a sample to 80 °C for an hour, consistent with the rigidity of the disphenoidal frame inferred for $[\mathbf{6P}]^{3+}$ from ^1H NMR spectroscopy (Fig. 4).

Addition of excess Cl_2 gas to MeCN solution of $[6'P][OTf]_3$ yields a product with identical spectral features as those assigned to $[(tbbipy)_2PCl_2]^{3+}$, as well as a number of unidentified byproducts. Interestingly, equimolar mixtures of $[6'As][OTf]_3$ and SO_2Cl_2 showed no evidence of reaction even after heating to 80 °C for 2 hours. ^1H NMR assays of these reaction mixtures showed only signals due to unreacted $[6'As][OTf]_3$.

Conclusions

In summary, we have isolated and comprehensively characterized the bipyridine complexes $[\mathbf{6E}][OTf]_3$ and $[6'E][OTf]_3$ for E = P, As, Sb, Bi, representing rare examples of salts containing trications and unique homologous series. The solid-state structures show systematic variations as a function of the atomic size of E. Larger element centers facilitate interion interactions for $[\mathbf{6E}][OTf]_3$ and $[6'E][OTf]_3$ in the order E = P < As < Sb < Bi as determined by X-ray crystallography and infrared spectroscopy. Gas-phase calculations (PBE0/def2-TZVP) reveal a trend from polar covalent to ionic E–N bonds for $[\mathbf{6E}]^{3+}$ going from E = P to E = Bi, consistent with data from ^1H NMR spectroscopy. The Lewis acidity of monoatomic trications E^{3+} exhibits the trend E = Bi < Sb < As < P based on calculation of charge densities and ligand dissociation energies in the gas phase. However the calculated Lewis acidity of complexes $[\mathbf{6E}]^{3+}$ towards a prototypical ligand, $OPMe_3$, exhibit the opposite trend, E = P < As < Sb < Bi due to steric factors.

Derivatives of $[6'E][OTf]_3$ with E = P and As represent rare examples of non-metal triflates and $E(OTf)_3$ transfer reagents, as illustrated by reactions with dmap, which proceed *via* ligand displacement to yield $[(dmap)_3E][OTf]_3$ and free tbbipy. Reactions of $[6'E][OTf]_3$ with PR_3 give access to E^I-containing cations concomitant with oxidative P–P coupling. Cations $[6'E]^{3+}$ (E = P, As) are single-component C–H bond activating agents as shown by dehydrogenation of 1,4-cyclohexadiene, which occurs more rapidly for E = P than for E = As. Both cations also

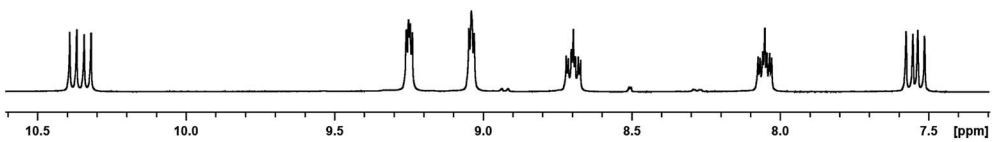

Fig. 6 Portion of the ^1H NMR spectrum (CD_3CN, 298 K) of the crude reaction mixture containing equimolar amounts of $[6'P][OTf]_3$ and SO_2Cl_2.

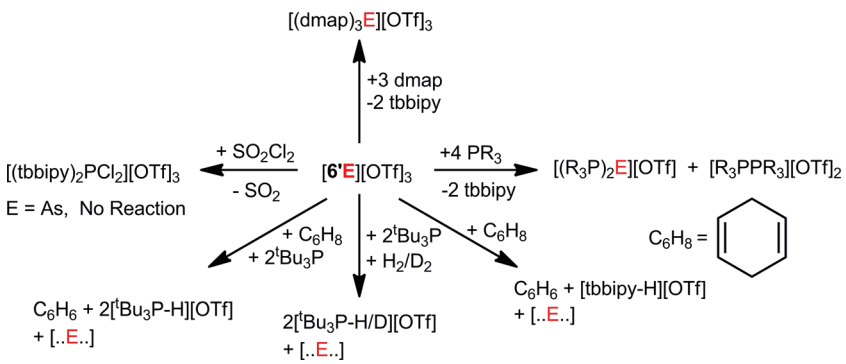

Scheme 6 Reactivity of $[6'E][OTf]_3$ (E = P, As).

dehydrogenate 1,4-cyclohexadiene in the presence of $^{t}Bu_3P$, indicative of frustrated Lewis pair chemistry. Combinations of $[\mathbf{6'E}][OTf]_3$ (E = P, As) with $^{t}Bu_3P$ activate H_2 or D_2 under mild conditions to give $[^{t}Bu_3P\text{-}H/D]^{1+}$. While the reaction of $[\mathbf{6'P}][OTf]_3$ with SO_2Cl_2 furnished the P^{V}-containing $[(tbbipy)_2PCl_2][OTf]_3$, the analogous oxidation of $[\mathbf{6'As}][OTf]_3$ was not observed. These observations highlight a rich reaction chemistry for $P(OTf)_3$ and $As(OTf)_3$ (Scheme 6) that is rendered accessible in salts $[\mathbf{6E}][OTf]_3$ and $[\mathbf{6'E}][OTf]_3$.

Acknowledgements

We thank the Natural Sciences and Engineering Research Council (NSERC) of Canada and the Vanier Canada Graduate Scholarships Program for funding. We thank the referees for their valuable suggestions regarding additional reactivity studies of $[\mathbf{6'E}][OTf]_3$.

References

1 J. L. Dutton and P. J. Ragogna, *Coord. Chem. Rev.*, 2011, **255**, 1414–1425.
2 S. S. Chitnis, Y. Carpenter, N. Burford, R. McDonald and M. J. Ferguson, *Angew. Chem., Int. Ed.*, 2013, **52**, 4863–4866.
3 S. S. Chitnis, A. P. M. Robertson, N. Burford, J. J. Weigand and R. Fischer, *Chem. Sci.*, 2015, **6**, 2559–2574.
4 I. Vargas-Baca, M. Findlater, A. Powell, K. V. Vasudevan and A. H. Cowley, *Dalton Trans.*, 2008, 6421–6426.
5 (*a*) J. J. Weigand, K. Feldmann, A. K. C. Echterhoff, A. W. Ehlers and K. Lammertsma, *Angew. Chem., Int. Ed.*, 2010, **49**, 6178–6181; (*b*) L. Gu, G. Gopakumar, P. Gualco, W. Thiel and M. Alcarazo, *Chem.–Eur. J.*, 2014, **20**, 8575–8578.
6 (*a*) J. Petuskova, M. Patil, S. Holle, C. W. Lehmann, W. Thiel and M. Alcarazo, *J. Am. Chem. Soc.*, 2011, **133**, 20758–20760; (*b*) F. D. Henne, A. T. Dickschat, F. Hennesdorf, K.-O. Feldmann and J. J. Weigand, *Inorg. Chem.*, 2015, **54**, 6849–6861.
7 R. Garbe, B. Vollmer, B. Neumüller, J. Pehler and K. Dehnicke, *Z. Anorg. Allg. Chem.*, 1993, **619**, 271–276.
8 Preliminary communication: S. S. Chitnis, N. Burford and M. J. Ferguson, *Angew. Chem., Int. Ed.*, 2013, **52**, 2042–2045.
9 S. Kobayashi, M. Sugiura, H. Kitagawa and W. W. L. Lam, *Chem. Rev.*, 2002, **102**, 2227–2302.
10 I. Tsuneo, Y. Koide and S. Hiyama, *Chem. Lett.*, 1990, **19**, 1445–1446.
11 R. Corbo, T. P. Pell, B. D. Stringer, C. F. Hogan, D. J. D. Wilson, P. J. Barnard and J. L. Dutton, *J. Am. Chem. Soc.*, 2014, **136**, 12415–12421.
12 M. Donath, M. Bodensteiner and J. J. Weigand, *Chem.–Eur. J.*, 2014, **20**, 17306–17310.
13 C. D. Martin, C. M. le and P. J. Ragogna, *J. Am. Chem. Soc.*, 2009, **131**, 15126–15127.
14 J. Beckmann, J. Bolsinger, A. Duthie, P. Finke, E. Lork, C. Lüdtke, O. Mallow and S. Mebs, *Inorg. Chem.*, 2012, **51**, 12395–12406.
15 P. A. Rupar, V. N. Staroverov and K. M. Baines, *Science*, 2008, **322**, 1360–1363.
16 C. L. B. Macdonald, A. M. Corrente, C. G. Andrews, A. Taylor and B. D. Ellis, *Chem. Commun.*, 2004, 250–251.
17 N. Li, R. Qiu, X. Zhang, Y. Chen, S. Yin and X. Xiu, *Tetrahedron*, 2015, **71**, 4275–4281.
18 J. B. Hendrickson and M. S. Hussoin, *J. Org. Chem.*, 1987, **52**, 4137–4139.
19 S. Kobayashi and I. Komoto, *Tetrahedron*, 2000, 6463–6465.
20 H. Gaspard-Iloughmane and C. le Roux, *Eur. J. Org. Chem.*, 2004, 2517–2532.
21 S. S. Chitnis, A. P. M. Robertson, N. Burford, J. J. Weigand and R. Fischer, *Chem. Sci.*, 2015, **6**, 2559–2574.
22 M. Peyronneau, C. Arrondo, L. Vendier, N. Roques and C. le Roux, *J. Mol. Catal. A: Chem.*, 2004, **211**, 89–91.
23 λ_{max} = 300 nm for $[\mathbf{6'P}]^{3+}$. For model cation $[\mathbf{6P}]^{3+}$, time-dependent DFT (PBE0/def2-TZVP, acetonitrile field) calculations yield a λ_{max} of 366 nm corresponding to a HOMO–LUMO transition. See Fig. S1, ESI† for the experimental absorbance spectrum and views of the HOMO and LUMO in $[\mathbf{6P}]^{3+}$.
24 A. J. Arduengo III and C. A. Stewart, *Chem. Rev.*, 1994, **94**, 1215–1237.
25 P. Pyykkö and M. Atsumi, *Chem.–Eur. J.*, 2009, **15**, 186–197.
26 A. Bondi, *J. Phys. Chem.*, 1964, **68**, 441–451.
27 M. Mantina, A. C. Chamberlin, R. Valero, C. J. Cramer and D. G. Truhlar, *J. Phys. Chem. A*, 2009, **113**, 5806–5812.
28 D. H. Johnston and D. F. Shriver, *Inorg. Chem.*, 1993, **32**, 1045–1047.
29 G. A. Olah, O. Farooq, C. X. Li, M. A. M. F. Farnia and J. J. Aklonis, *J. Appl. Polym. Sci.*, 1992, **45**, 1355–1360.
30 M. E. Woordhouse, F. D. Lewis and T. J. Marks, *J. Am. Chem. Soc.*, 1982, **104**, 5586–5594.
31 V. Gutmann, *Coord. Chem. Rev.*, 1976, **18**, 225–255.
32 M. A. Beckett, G. C. Strickland, J. R. Holland and K. S. Varma, *Polymer*, 1996, **37**, 4629–4631.
33 Derivatives of $[\mathbf{6'E}][OTf]_3$ were used since the poor solubility of $[\mathbf{6P}][OTf]_3$ makes ^{31}P NMR measurements challenging.
34 M. H. Holthausen, R. R. Hiranandani and D. W. Stephan, *Chem. Sci.*, 2015, **6**, 2016–2021.
35 A. E. Ashley, T. J. Herrington, G. C. Wildgoose, H. Zaher, A. L. Thompson, N. H. Rees, T. Krämer and D. O'Hare, *J. Am. Chem. Soc.*, 2011, **133**, 14727–14740.
36 K. Schwedtmann, M. H. Holthausen, K.-O. Feldmann and J. J. Weigand, *Angew. Chem., Int. Ed.*, 2013, **52**, 14204–14208.
37 G. Muller, H. Matheus and M. Winkler, *Z. Naturforsch., B: J. Chem. Sci.*, 2001, **56**, 1155–1162.
38 P. Wawrzyniak, A. L. Fuller, A. M. Z. Slawin and P. Kilian, *Inorg. Chem.*, 2009, **48**, 2500–2506.
39 I. Granoth and J. C. Martin, *J. Am. Chem. Soc.*, 1979, **101**, 4623–4626.
40 A. N. Kornev, V. V. Sushev, Y. S. Panova, N. V. Zolotareva, E. V. Baranov, G. J. Fukin and G. A. Abakumov, *Eur. J. Inorg. Chem.*, 2015, 2057–2066.
41 K.-O. Feldmann and J. J. Weigand, *Angew. Chem., Int. Ed.*, 2012, **51**, 6566–6568.

42 E. Conrad, N. Burford, U. Werner-Zwanziger, R. McDonald and M. J. Ferguson, *Chem. Commun.*, 2010, **46**, 2465–2467.
43 A. L. Brazeau, A. S. Nikouline and P. J. Ragogna, *Chem. Commun.*, 2011, **47**, 4817–4819.
44 S. G. Baxter, A. H. Cowley and S. K. Mehrotra, *J. Am. Chem. Soc.*, 1981, **103**, 5572–5573.
45 N. Burford, T. M. Parks, B. W. Royan, B. Borecka, T. S. Cameron, J. F. Richardson, E. J. Gabe and R. Hynes, *J. Am. Chem. Soc.*, 1992, **114**, 8147–8153.
46 C. Hering, J. Rothe, A. Schulz and A. Villinger, *Inorg. Chem.*, 2013, **52**, 7781–7790.
47 K.-O. Feldmann and J. J. Weigand, *Angew. Chem., Int. Ed.*, 2012, **51**, 7545–7549.
48 J. Carreras, M. Patil, W. Thiel and M. Alcarazo, *J. Am. Chem. Soc.*, 2012, **134**, 16753–16758.
49 R. Weiss and S. Engel, *Synthesis*, 1991, **12**, 1077–1079.
50 R. Weiss and S. Engel, *Angew. Chem., Int. Ed.*, 1993, **31**, 216–217.
51 L. V. Bezgubenko, S. E. Pipko and A. D. Sinista, *Russ. J. Gen. Chem.*, 2009, **79**, 911–918.
52 We note that the crystal structure of [**7P**][OTf]$_3$ was previously presented by M. Donath, K. Schwedtmann, A. K. C. Echterhoff, R. Panzer, S. Schulz, F. Hennesdorf, and J. J. Weigand, at the International Conference on Sustainable Phosphorus Chemistry (ICSPC), Florence, December 04, 2014.
53 S. S. Chitnis, E. MacDonald, N. Burford, U. Werner-Zwanziger and R. McDonald, *Chem. Commun.*, 2012, **48**, 7359–7361.
54 J. J. Weigand, S. D. Riegel, N. Burford and A. Decken, *J. Am. Chem. Soc.*, 2007, **129**, 7969–7976.
55 A. Schmidpeter, S. Lochschmidt and W. S. Sheldrick, *Angew. Chem., Int. Ed.*, 1985, **24**, 226–227.
56 J. M. McBride, *Tetrahedron*, 1974, 2009–2022.
57 B. D. Ellis and C. L. B. MacDonald, *Inorg. Chem.*, 2004, **43**, 5981–5986.
58 M. H. Holthausen, J. M. Bayne, I. Mallov, R. Dobrovetsky and D. W. Stephan, *J. Am. Chem. Soc.*, 2015, **137**, 7298–7301.
59 D. W. Stephan, *Acc. Chem. Res.*, 2015, **48**, 306–316.
60 S. E. Pipko, L. Bezgubenko, A. D. Sinista, E. B. Rusanov, E. G. Kapustin, M. I. Povolotskii and V. V. Schvadchak, *Heteroat. Chem.*, 2008, **19**, 171–177.
61 K. B. Dillon, R. N. Reeve and T. Waddington, *J. Chem. Soc., Dalton Trans.*, 1977, 2382–2388.